Indian Journal of Chemistry
Vol. 59A, September 2020, pp. 1298-1304

Optoelectronic properties of all-Inorganic lead-free halide double perovskites $(Rb_xCs_{1-x})_2AgBiBr_6$ for solar cell applications

R Radhakrishnan

Department of Theoretical Physics, University of Madras, Chennai-600 025, Tamil Nadu, India

*E-mail: rkrishna.tp@gmail.com

Received 04 April 2020; *accepted 31 July 2020*

Solar cells based on lead-free double perovskites as absorber layer is an environment friendly, stable alternative for the conventional lead based hybrid halide perovskites. A comprehensive theoretical study on the optical and electronic properties of all-inorganic double perovskite with $A_2BB'X_6$ stoichiometry is done using density functional theory. Doping studies on $(Rb_xCs_{1-x})_2AgBiBr_6$ perovskite is done using the virtual crystal approximation method within density functional theory. It is found that as increasing the Rb content (x) from 0.0 to 1.0 in $Rb_xCs_{1-x}AgBiBr_6$, the lattice parameter, dielectric constant and band gap are found to be decreasing linearly in accordance with Vegard's law. The lattice constant decreases linearly in x with a function of $a(x) = 11.516 - 0.0057\ x$ (Å), while the band gap decreases linearly as a function of x, $E_g(x) = 1.472 - 0.0009\ x$ (eV). Opto-electronic properties of substitutional doping of Rb in $(Rb_xCs_{1-x})_2AgBiBr_6$ is compared with Cs_2AgBiX_6 (X=Cl, Br, I) and Br doped $Cs_2AgIn(Br_xCl_{1-x})_6$.

Keywords: DFT, Double Perovskites, Halide Doping, Solar cells

Solar cells based on hybrid organic inorganic perovskite (HOIP) materials have been a topic of great interest in recent years. Perovskite solar cells have reached power conversion efficiency (PCE) of 25.2% in a decade's time[1,2]. This exceptional PCE arises from the opto-electronic properties of semiconducting halide perovskites, namely a high optical absorption coefficient (25 times higher than that of silicon), a tunable band gap (over a wide range of electromagnetic spectrum), long carrier recombination lifetimes, long diffusion lengths (~750 μm) and a high electron/hole mobility and transmission quality with small exciton binding energy and electron/hole effective masses[3-6]. These properties lead to an optimal utilization of absorbed solar photons within the active perovskite layer. Thus, HOIP hold the highest efficiencies ever achieved from a solution processable material. HOIP in particular methylammonium $(CH_3NH_3)^+$) and formamidinium $(CH_3(NH_2)^{2+}$) lead iodides and similar compounds with their outstanding properties have been considered as the "first high-quality halide semiconductors". HOIP have many advantages over the conventional semiconductor-based photo voltaic devices, but the toxicity of lead and compound stability are the two main challenges[7-10]. Extensive studies have been performed in the last seven years on this emerging photo-voltaics and have found improved performance of perovskite opto-electronic devices. Replacing or mixing cations (organic molecules) in HOIP with inorganic Cs or Rb has been reported to increase the material stability[11,12]. Among various All-inorganic cesium lead halide perovskites $(CsPbX_3)$, $CsPbI_3$ is regarded as a promising all-inorganic perovskite with a band gap of 1.73 eV with an efficiency (18.4%)[14-17]. It was found that all-inorganic double perovskites Cs_2AgBiX_6 are more stable and are the best environment friendly alternatives to lead-halide perovskites[19-26].

Substitution of A site with different isovalent species reduces the efficiency. Theoretical screening of the compounds where Pb replaced by other isovalent elements resulted in non-ideal band gaps[27,28]. For instance, it is shown that by different combination of halides and cations the electronic properties can be tuned[-19-31]. Chemical doping of alkaline earth metals, constructing perovskite bilayer architectures, using two-dimensional perovskites and vacancy/cation ordered double perovskites, including hybrid halide double perovskites (HHDP), all inorganic halide double perovskites (AIHDP) are few strategies to improve the efficiency of PSCs[32-39]. Environment friendly stable and non-toxic AIHDP

with chemical formula $A_2BB'X_6$ (where *B=Ag, Cu; B'=Bi, Sb, In*) have indirect and wide band gaps of over 2 eV. Among the various lead-free HDP, compounds based on In and Ag have direct band gap[29,30,36-39].

In this work, the effect of doping on the structural, electronic and optical properties of all-inorganic perovskites $(Rb_xCs_{1-x})_2AgBiBr_6$ were compared using density functional theory (DFT). Similarly, the effect of doping of Rb in all-inorganic double perovskites $Cs_2AgBiBr_6$ *(X=Cl,Br,I)* have also been investigated. The basic electronic properties have been analyzed in terms of the band structure and density of states. Partial densities of states of the pure and doped materials were obtained to evaluate the contributions of specific orbitals to the valence and conduction bands. For a comparative study, frequency dependent absorption coefficient was used in our simulation. The real and imaginary parts of the dielectric constant were also analyzed separately.

Computational details and Results

For the current work, geometry optimizations, electronic and optical studies were done using the Quantum- Espresso (QE) suite[44]. The exchange–correlation function with generalized gradient approximation (GGA) parametrized by Perdew Burke Ernzerhof (PBE) was used[45]. All the structures were optimized theoretically using the Birch-Murnaghan's equation of state. The convergence test for kinetic energy cut-off for wave function (ecutwfc) and charge densities (ecutrho) were done and ecutwfc was set to 90 while ecutrho was set to 720 Ry. Structure optimization and the k-point meshes for different structures were done according to the Monkhorst–Pack scheme for the Brillouin zones[46]. Sampling of Brillouin zone integration with k-point mesh 8×8×8 was set, for DOS and optical calculations denser k-mesh of 16×16×16 was used.

Structural Properties

The AIHDP $Cs_2BB'X_6$ was modelled in a cubic double perovskite structure with space group *Fm3m(#225)*. The structure is an arrangement of corner-sharing BX_6 and $B'X_6$ units which consist of two types of octahedra, alternating in a rock-salt face-centered cubic structure. The conventional structure of $Cs_2BB'X_6$ is given in Fig. 1C. The fractional coordinates of the *Ag, Bi* and *Cs* atoms are (*0.0, 0.0, 0.0*), (*0.5, 0.5, 0.5*) and (*0.25, 0.25, 0.25*) with Wyckoff position *4a, 4b* and *8c*, respectively. In Table 1, the lattice parameters and corresponding tolerance factor of $Cs_2BB'X_6$ double perovskites are presented. As seen in the table, Goldschmidt tolerance factor (τ) was observed to be in the proximity of one, which is

Table 1 — Lattice parameter of various potential cesium based double perovskites compared along with its calculated tolerance factors

	X	Lattice Constant (Å)	Tolerance Factor (τ)
Cs_2AgBiX_6	*Br*	*11.4728*[19]	*0.9539*[19]
	Cl	*10.9788*[19]	*0.9559*[19]
Cs_2CuBiX_6	*Br*	*11.0928*	*0.9866*
	Cl	*10.5148*	*0.9981*
Cs_2AgInX_6	*Br*	*11.2711*[29,30]	*0.9710*[29,30]
	Cl	*10.5788*[29,30]	*0.9920*[29,30]
Cs_2CuSbX_6	*Br*	*10.9188*	*1.0023*
	Cl	*10.2548*	*1.0234*
Cs_2AgSbX_6	*Br*	*11.2988*	*0.9686*
	Cl	*10.7188*	*0.9791*
Cs_2CuInX_6	*Br*	*10.8911*	*1.0049*
	Cl	*10.1148*	*1.0375*
Cs_2AuBiX_6	*Br*	*10.8599*	*1.0078*
	Cl	*10.3259*	*1.0163*

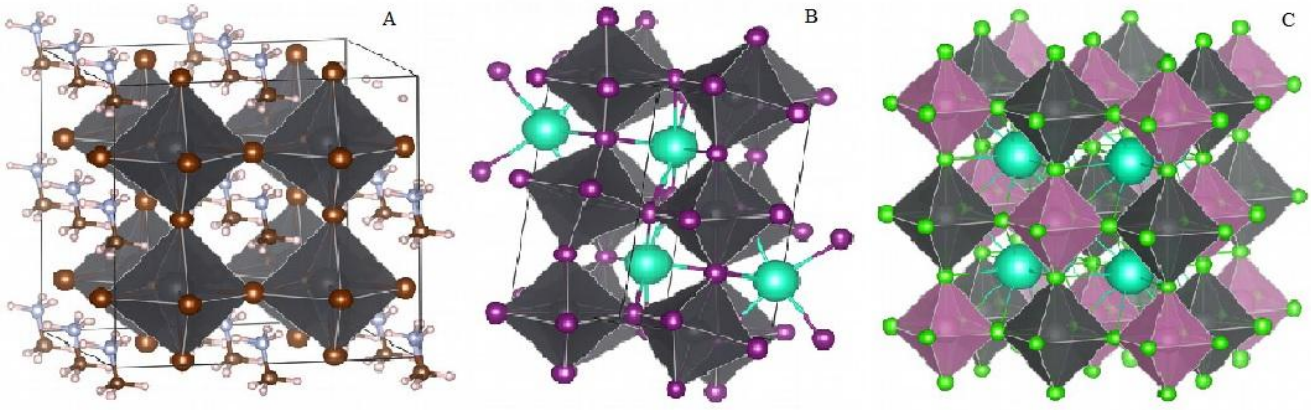

Fig. 1 — Crystal structures of most commonly used halide perovskites. (A) $CH_3NH_3^+$ PbI_3 with space group *Pmm(#221)*, (B) Orthorombic $CsPbI_3$ with space group *Pbnm(#62)*, and (C) $Cs_2AgBiCl_6$ with space group *Fmm(#225)*. Pictures generated using VESTA

considered to form stable cubic perovskite structures. Structural optimization of $(Rb_xCs_{1-x})_2AgBiBr_6$ was done with PBE exchange functional. The volume optimization was performed using the Birch-Murnaghan's equation of state. The lattice constants of the compounds were first optimized by estimating the Energy−Volume data and then fitting it into the Birch-Murnaghan Equation of State (EOS) which is given by

$$E(V) = E_0 + \frac{9V_0B_0}{16}\{[(\frac{V_0}{V})^{\frac{2}{3}} - 1]^3 B_0' + [(\frac{V_0}{V})^{\frac{2}{3}} - 1]^2[6 - 4(\frac{V_0}{V})^{\frac{2}{3}}]\}.$$

where, E is internal energy, B_0 is the bulk modulus, B_0' is the derivative of the bulk modulus with respect to pressure, V_0 is the reference volume and V is the deformed volume. Optimized values of the parameters of Birch-Murnaghan's EOS for $Rb_{0.2}Cs_{0.8}AgBiBr_6$ and $Rb_2AgBiBr_6$ are presented in Fig. 2. For $Rb_2AgBiBr_6$ the values of optimized lattice parameters a, B_0, B'_0 and V_0 were *21.6548*, *233* kbar, *5.17* and *2538.66* (a.u.)^3, respectively. Similarly, the corresponding values for $Rb_{0.2}Cs_{0.8}AgBiBr_6$ were *21.7416* a.u., B_0 = *240* kbar, B'_0 = *5.95* and V_0 = *2569.31* (a.u.)^3, respectively. As expected there was a variation in the lattice constant due to the doping of Rb and was compared with other compounds in Table 2. This variation follows Vgard's law with a linear function *a(x) = 11.516 - 0.0057 x* (Å), where *x* is the Rb content in the compound.

Electronic properties

Band structure calculations for Cs_2AgBiX_6 using LDA, PBE and PBE sol exchange correlation have been extensively investigated along with the spin-orbit coupling earlier[19]. The band gaps for $Cs_2AgBiCl_6$, $Cs_2AgBiBr_6$ and Cs_2AgBiI_6 are 1.91 eV, 1.42 eV and 0.89 eV, respectively in PBE-GGA approximation. Band gap was found to be indirect with the valence band maximum (VBM) at X and the conduction band minimum (CBM) at L points of the Brillouin zone. The band structures of Cs_2AgBiX_6 through high symmetry points are shown in Fig. 3. It is to be noted that among various *Cs* based double halides, band gap of $Cs_2AgInCl_6$ was found to be direct[40-43], with the VBM and CBM at $\Gamma(\pi/a\ ,\ \pi/a\ ,\ \pi/a)$ point of the Brillouin zone[29,30]. The calculated band gap for $Cs_2AgInCl_6$ was obtained as 1.1 eV. Similarly, the structural, electronic and optical properties of bromine (Br) doped $Cs_2AgInCl_6$ in the cubic phase (*Fm3m#225*) have also been investigated by our group already[29,30].

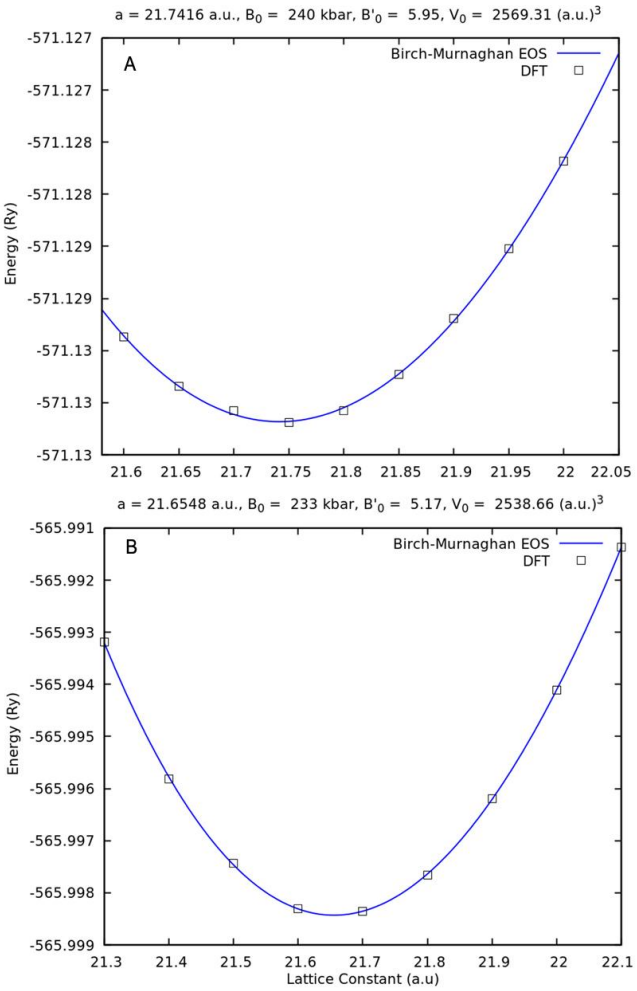

Fig. 2 — Optimized values of the parameters of Birch-Murnaghan's equation of state are presented for (A) $Rb_{0.2}Cs_{0.8}AgBiBr_6$ and (B) $Rb_2AgBiBr_6$. (Plots genarated using Gnuplot)

Table 2 — Lattice parameters and Bandgaps of double perovskites $(Rb_xCs_{1-x})_2AgBiBr_6$ compared with Cs_2AgBiX_6 $(X=Cl,Br,I)$[19] and direct band gap $Cs_2AgIn(Br_xCl_{1-x})_6$[29-30].

Compound	Lattice Constant (Å)	Bandgap (eV)
$Cs_2AgBiCl_6$	*10.9788* [19]	1.91[19]
$Cs_2AgBiBr_6$	*11.4728* [19]	1.4233 [19]
Cs_2AgBiI_6	12.2843 [19]	0.89 [19]
$Cs_2AgInCl_6$	*10.5788* [29-30]	1.1 [29-30]
$Cs_2AgIn(Br_{0.04}\ Cl_{0.96})_6$	10.563 [30]	1.033[30]
$Cs_2AgIn(Br_{0.08}\ Cl_{0.92})_6$	10.597[30]	1.016[30]
$Cs_2AgIn(Br_{0.12}\ Cl_{0.88})_6$	10.606[30]	0.995[30]
$Cs_2AgIn(Br_{0.16}\ Cl_{0.84})_6$	10.612[30]	0.944[30]
$(Rb_{0.2}Cs_{0.8})_2AgBiBr_6$	11.50518	1.4709
$(Rb_{0.4}Cs_{0.6})_2AgBiBr_6$	11.49270	1.469
$(Rb_{0.6}Cs_{0.4})_2AgBiBr_6$	11.48122	1.4672
$(Rb_{0.8}Cs_{0.2})_2AgBiBr_6$	11.47081	1.4656
$Rb_2AgBiBr_6$	11.45924	1.4634

For the doping percentages of 4, 8, 12 and 16%, the lattice constants and band gap were found to be

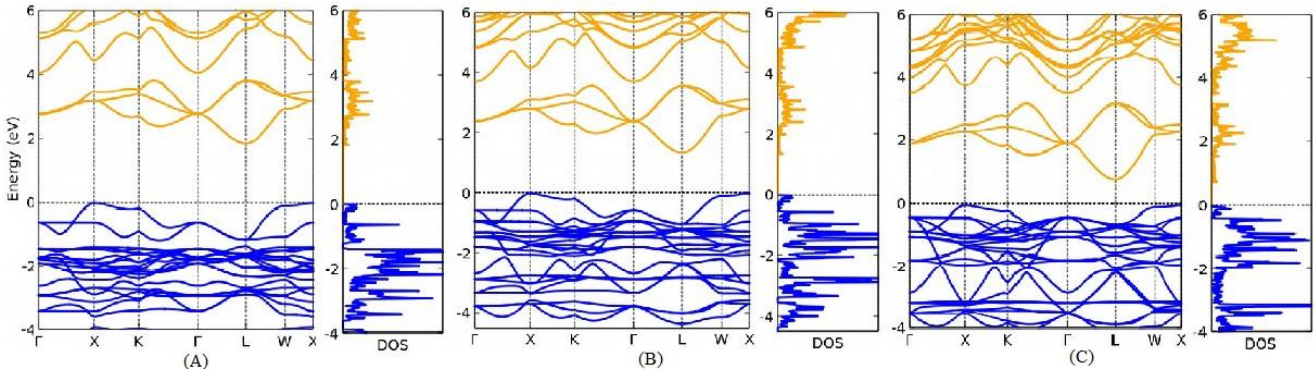

Fig. 3 — Electronic band structure and DOS of Cs_2AgBiX_6. along high symmetry points. Zero set to VBM (A) $Cs_2AgBiCl_6$; (B) $Cs_2AgBiBr_6$; and (C) Cs_2AgBiI_6

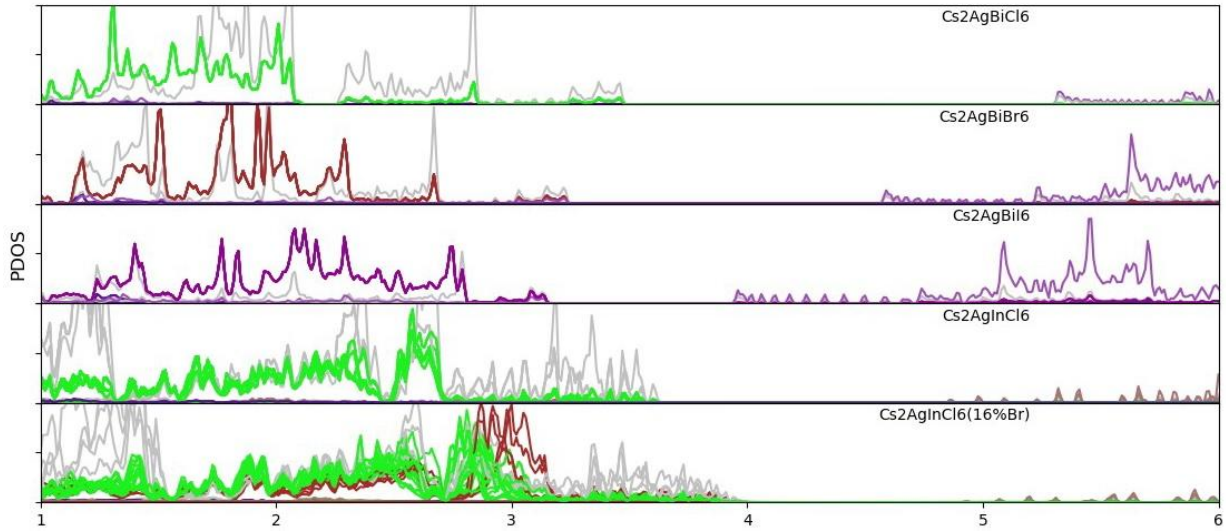

Fig. 4 — Atom-projected partial DOS showing the variations in the electronic configurations as B-cations and halides are changed

10.563 Å, 10.597 Å, 10.606 Å, 10.612 Å and 1.033 eV, 1.016 eV, 0.995 eV, 0.944 eV, respectively. Further, to investigate the contribution of various atoms to the valance and conduction band, we have plotted the atom-projected partial DOS. The variation tendency in electronic structures was studied by obtaining partial density of states (PDOS) projected on each atom (Fig. 4).

Electronic structure calculations of $(Rb_xCs_{1-x})_2AgBiBr_6$ $(0<x<1)$ using VCA method shows that electronic properties are not affected by the Rb doping. Lattice constant and band gap as a function of Rb content x is presented in Table 2. When increasing the Rb content x from 0.0 to 1.0, band gap decreases linearly as a function of doping content x as $E_g(x) = 1.472 - 0.0009\ x$ (eV) with χ^2 =9.8*10^{-08}. These results are summarised in Fig. 5B. Here the slope is very small (*0.0009*) which shows that the effect of A cation doping is practically negligible in the context of electronic properties. The effect of changing the halide configurations on electronic properties is more prominent than due to the doping of Rb as shown in Table 2 and in Fig. 3.

Optical properties

The frequency dependent photo-absorption coefficient is a major optical property that determines the sensitivity of the material towards the incident solar energy. The studied electronic properties reveal that these compounds are suitable for photovoltaic applications. The response of the incident frequency ω to the absorption coefficient $\alpha(\omega)$ and refractive index $n(\omega)$ are expressed in terms of permittivity ε as $\alpha(\omega) = \omega/cn(\omega)$ where c is the speed of light and

$$n(\omega) = \frac{1}{\sqrt{2}}\left(\sqrt{\varepsilon_R(\omega)^2 + \varepsilon_I(\omega)^2} + \varepsilon_R(\omega)\right)^{\frac{1}{2}}.$$

Here, $\varepsilon_R(\omega)$ and $\varepsilon_I(\omega)$ are the real and imaginary

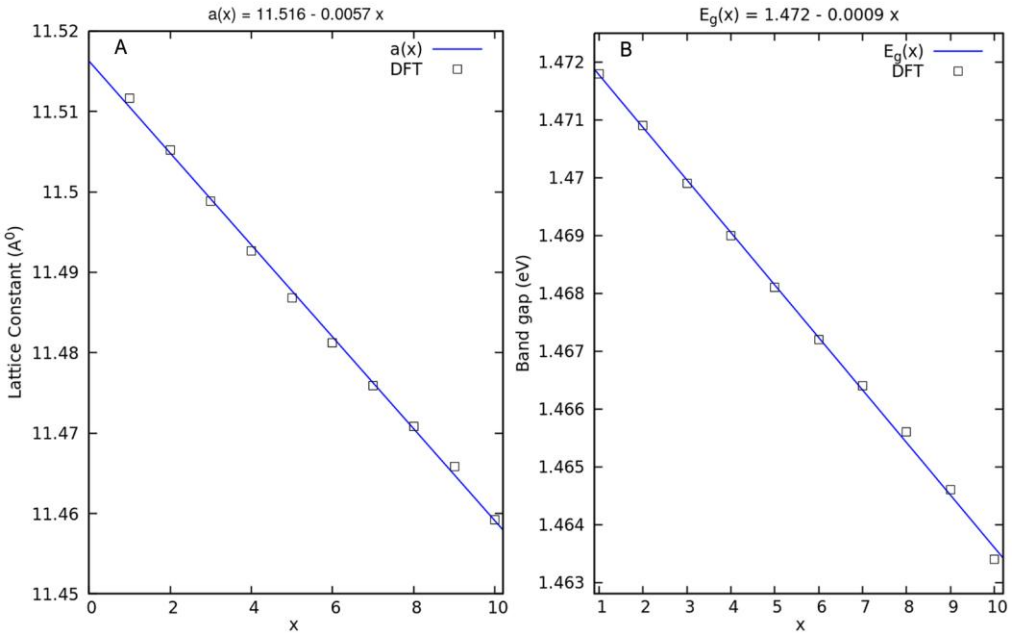

Fig. 5 — Variations of (A) Lattice constant; and (B) Band gap of $(Rb_xCs_{1-x})_2AgBiBr_6$ as a function of Rb content *x*, calculated using the VCA method within DFT. (Plots genarated using Gnuplot)

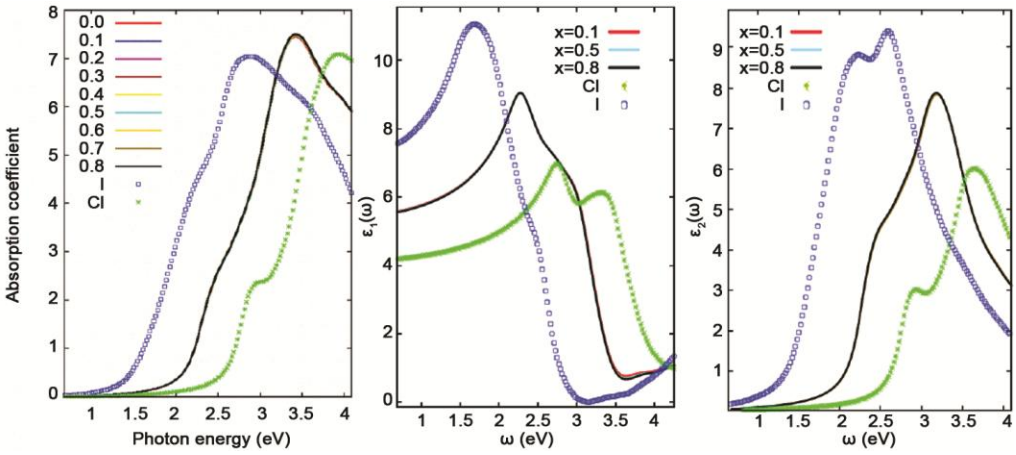

Fig. 6 — Absorption and dielectric constant for *Rb* doped $CS_2AgBiBr_6$ compared with Cs_2AgBiX_6 *(X=Cl,Br,I)*[19] as a function of photon energy. (A) Absorption coefficient of $(Rb_xCs_{1-x})_2AgBiBr_6$ compared with $CS_2AgBiCl_6$ [19] and CS_2AgBiI_6 [19], (B) Real part of the dielectric constant, and (C) Imaginary part of dielectric constant compared with Rb doped $CS_2AgBiBr_6$. (Plots genarated using Gnuplot)

parts of the dielectric constant $\varepsilon(\omega) = \varepsilon_R + i\varepsilon_I$. The frequency-dependent dielectric constants, $\varepsilon(\omega)$ were calculated within the density functional perturbation theory as implemented in the QE package. In Fig. 6A, the absorption coefficient (α) as a function of incident photon energy (ω) for $(Rb_xCs_{1-x})_2AgBiBr_6$ were compared with $Cs_2AgBiX_6(X=Cl,Br,I)$[19] showing the effect of changes in A-cation and halogen. Optical properties are not affected by the Rb doping but can be tuned by changing the halogen configurations. From the absorption spectra it is observed that these materials can be used as light absorber in silicon tandem solar cells.

Conclusions

In this study, the structural, electronic and optical properties were investigated using first-principles density functional theory for a class of double perovskites. Theoretically, efficient inorganic halide PSCs were designed which are environment friendly as well as stable alternative to lead halide perovskites. Further, the compounds $Cs_2AgBiX_6(X=Cl,Br,I)$,

$Cs_2AgIn(Br_xCl_{1-x})_6$ and $(Rb_xCs_{1-x})_2AgBiBr_6$ were also analyzed. This comprehensive theoretical work compares the effect of doping at A site and also the effect of halogen doping on the double perovskite $A_2BB'X_6$. A few candidates for AIHDPs with chemical formula $A_2BB'X_6$ were constructed which are stable compounds thereby making them a potential candidate for photovoltaic applications. Different percentages of Rb doping done at *A*-site showed that these compounds have similar optical properties with increased structural stability. In this work, virtual crystal approximation method was used to investigate the influence of doping at A site of halide perovskites $(Rb_xCs_{1-x})_2AgBiBr_6$. ($0.0 < x < 1.0$), and it was found that the lattice constants decreases with increased x and follows the Vegard's law, with the linear function of x as $a(x) = 11.516 - 0.0057\ x$ (Å). Similarly, the band gap also decreased linearly as a function of x. Electronic properties showed AIHDPs Cs_2AgBiX_6 and Rb doped $(Rb_xCs_{1-x})_2AgBiBr_6$ has indirect band gap and $Cs_2AgInCl_6$ has direct band gap. The band gap of $Cs_2AgInCl_6$ was 1.1eV with the VBM and CBM at Γ point of the Brillouin zone. As the doping percentage of Br in $Cs_2AgInCl_6$ was increase to 16%, the band gap got reduced to 0.9 eV. From the optical studies, it could be concluded that along with stable AIHDPs Cs_2AgBiX_6, Rb doped $Cs_2AgIn(Br_xCl_{1-x})_6$ and $(Rb_xCs_{1-x})_2AgBiBr_6$ are strong candidates for potential applications in photovoltaic technologies.

Acknowledgment

Author would like to acknowledge PARAM Yuva supercomputing facility at Centre for Development of Advanced Computing (C-DAC), Pune, India for extending the support. All plots were generated using gnuplot (http://www.gnuplot.info/).

Conflict of interest

The authors declare no conflict of interests in this study.

References

1 Kojima A, Teshima K, Shirai Y & Miyasaka T, *J Am Chem Soc*, 131 (2009) 6050.
2 Research Cell Efficiency Records National Renewable Energy Laboratory. https://www nrel gov/pv/assets/images/ efficiency-chart png. (Accessed September 17, 2020).
3 Stoumpos CC, Malliakas CD & Kanatzidis MG, *Inorg Chem*, 52 (2013) 9019.
4 McGehee MD, *Nat Mater*, 13 (2014) 845.
5 Lee MM , Teuscher J, Miyasaka T, Murakami TN & Snaith HJ, *Science*, 338 (2012) 643.
6 Demic S, Ozcivan AN, Can M, Ozbek C & Karakaya M, In: *Nanostructured Solar Cells;* (Ed. Das N; Intech: Rijeka, Croatia), 2017, pp 277.
7 Green M, Ho-Baillie A & Snaith HJ, *Nat Photonics*, 8 (2014) 506.
8 Li B, Li Y, Zheng C & Gao D, *RSC Adv*, 6 (2016) 38079.
9 Asghar MI, Zhang J, Wang H & Lund PD, *Renew Sustain Energy Rev*, 77 (2017) 131.
10 Ahmed ME, Ahmed ES, Sajid S, Mohamed MR, Ali MH & Meicheng L, *ACS Appl Mater Interfaces*, 10 (2018) 11699.
11 Xiaoming L, Fei C, Dejian Y, Jun C, Zhiguo S, Yalong S, Ying Z, Lin W, Yi W, Ye W & Haibo Z, *Small*, 13 (2017) 1603996.
12 Walsh A, *J Phys Chem C*, 119 (2015) 5755.
13 Michael S, Taisuke M, Konrad D, Ji YS, Amita U, Shaik MZ, Juan PCB, Wolfgang RT, Antonio A, Anders H & Michael G, *Science*, 354 (2016) 206.
14 Yong W, Ibrahim D, Luis KO, Taiyang Z, Miao K, Yawen L, Lijun Z, Xingtao W, Yingguo Y, Xingyu G, Yabing Q, Michael G & Yixin Z, *Science*, 365 (2019) 591.
15 Keqiang C, Wei J, Yupeng Z, Tingqiang Y, Peter R, Qiaohui Z, Udo B, Qitao L, Yingwei W, Han Z, Qiaoliang B & Yueli L, *J Am Chem Soc*, 8 (2020) 3775.
16 Kang W, Zhiwen J, Lei L, Hui B, Dongliang B, Haoran W, Jingru Z, Qian W & Shengzhong L, *Nat Commun*, 9 (2018) 4544.
17 Cho FJL, Zhiping W, Nobuya S, Jianghui Z, Chwen HL, Martin G, Shujuan H, Henry JS & Anita HB, *Adv Energy Mater*, 9 (2019) 1901685.
18 Cheng L, Yi Y, Xin L, Yong D, Zulqarnain A, Xinye L, Yuanlong L, Zian Z, Songyuan D & Mohammad KN, *J Mater Chem A*, 8 (2020) 10226.
19 Kumar NR, Radhakrishnan R, *Mater Lett*, (2018) 227.
20 Slavney AH, Hu T, Lindenberg AM & Karunadasa HI, *J Am Chem Soc*, 138 (2016) 2138.
21 McClure ET, Ball MR, Windl W & Woodward P M, *Chem Mater*, 28 (2016) 1348.
22 George V, Marina RF, Amir AH, Nobuya S, Bernard W, Henry JS & Feliciano G, *J Phys Chem Lett*, 7 (2016) 1254.
23 Filip MR, Hillman S, Haghighirad AA, Snaith HJ & Giustino F, *J Phys Chem Lett*, 7 (2016) 2579.
24 Savory CN, Walsh A, & Scanlon DO, *ACS Energy Lett*, (2016) 949.
25 Zhi JL, Elan H, Andrew HD, Alex K, Joshua TW, Boris D, Robert WM & Weiwei Z, *Chem Mater*, 30 (2018) 6400.
26 Gray MB, McClure ET & Woodward PM, *J Mater Chem C* 7 (2019) 9686.
27 Javier N, Antonio S, Juan JG, Norge CH, Jose CP, Rodrigo A, Concha F, Desireé S, Teresa A & Joaquín MC, *Nanoscale*, 7 (2015) 6216.
28 Aslihan B, Anitha E, Marc M & Bert C, *Nat Mater*, 15 (2016) 247.
29 Kumar N & Radhakrishnan R, *Mater Today*, 04 (2020) 233.
30 Nishitha M, Kumar NR & R Radhakrishnan, *Mater Today*, 03 (2020) 489.
31 Jacobsson TJ, Pazoki M, Hagfeldt A & Edvinsson T, *J Phys Chem C*, 119 (2015) 25673.
32 Filip MR, Eperon G, Snaith HJ & Giustino F, *Nat Commun*, 5 (2014) 5757.

33 David PM, Golnaz S, Waqaas R, Giles EE, Michael S, Maximilian TH, Amir H, Nobuya S, Lars K, Bernd R, Michael BJ, Laura MH & Henry JS, *Science*, 351 (2016) 151.

34 Körbel S, Marques MAL & Botti S, *J Mater Chem C*, 4 (2016) 3157.

35 Roknuzzaman Md, Chunmei Z, Kostya O, Aijun D, Hongxia W, Lianzhou W & Tuquabo T, *Sci Rep*, 9 (2019) 718.

36 George V, Amir AH, Rebecca LM, Weng HS, Marina RF, Bernard W, Michael BJ, Laura MH, Henry JS & Feliciano G, *J Phys Chem Lett*, 8 (2017) 772.

37 Wonseok L, Seunghwa H & Sungjee K, *J Phys Chem C*, 123 (2019) 2665.

38 Zhou J, Xia Z, Molokeev MS, Zhang X, Pend D & Liu Q, *J Mater Chem A*, 5 (2017) 15031.

39 Zhou J, Rong X, Molokeev MS, Zhang X, & Xia Z, *J Mater Chem A*, 6 (2018) 2346.

40 Tran TT, Panella JR, Chamorro JR, Morey JR & Mc-Queen TM, *Mater Horiz*, 4 (2017) 688.

41 Jiajun L, Xiaoming W, Shunran L, Jing L, Yueming G, Guangda N, Li Y, Yuhao F, Liang G, Qingshun D, Chunyi Z, Meiying L, Fusheng M, Wenxi L, Liduo W, Shengye J, Junbo H, Lijun Z, Joanne E, Jianbo W, Yanfa Y, Edward HS & Jiang T, *Nature*, 563 (2018) 541.

42 Jain A, Voznyy O & Sargent EH, *J Phys Chem C*, 121 (2017) 7183.

43 Fangyi Zhao, Zhen Song, Jing Zhao & Quanlin Liu, *Inorg Chem Front*, 6 (2019) 3621

44 Giannozzi P, Baroni S, Bonini N, Calandra M, Car R, Cavazzoni C, Ceresoli D, Chiarotti GL, Cococcioni M, Dabo I, Corso AD, Fabris S, Fratesi G, Gironcoli S, Gebauer R, Gerstmann U, Gougoussis C, Kokalj A, Lazzeri M, Martin-Samos L, Marzari N, Mauri F, Mazzarello R, Paolini S, Pasquarello A, Paulatto L, Sbraccia C, Scandolo S, Sclauzero G, Seitsonen AP, Smogunov A, Umari P & Wentzcovitch RM, *J Phys Condens Matter*, 21 (2009) 395502.

45 Giannozzi P, Andreussi O, Brumme T, Bunau O, Nardelli MB, Calandra M, Car R, Cavazzoni C, Ceresoli D, Cococcioni M, Colonna N, Carnimeo I, Corso AD, Gironcoli S, Delugas P, DiStasio RA, Ferretti A, Floris A, Fratesi G, Fugallo G, Gebauer R, Gerstmann U, Giustino, T Gorni, J Jia, M Kawamura, H-Y Ko, A Kokalj, E Küçükbenli, Lazzeri M, Marsili N, Marzari F, Mauri NL, Nguyen HV, Nguyen F, Otero-de-la-Roza A, Paulatto L, Poncé S, Rocca D, Sabatini R, Santra B, Schlipf M, Seitsonen AP, Smogunov A, Timrov I, Thonhauser T, Umari P, Vast N, Wu X & Baroni S, *J Phys Condens Matter*, 29 (2017) 465901.

46 Perdew JP, Ruzsinszky A, Csonka GI, Vydrov OA, Scuseria GE, Constantin LA, Zhou X & Burke K, *Phys Rev Lett*, 100 (2008) 136406.